On the Growth of Layers of Nonprecipitating Cumulus Convection

BJORN STEVENS

Department of Atmospheric and Oceanic Sciences, University of California, Los Angeles, Los Angeles, California

(Manuscript received 24 April 2006, in final form 13 November 2006)

ABSTRACT

A prototype problem of a nonprecipitating convective layer growing into a layer of uniform stratification and exponentially decreasing humidity is introduced to study the mechanism by which the cumulus-topped boundary layer grows. The problem naturally admits the surface buoyancy flux, outer layer stratification, and moisture scale as governing parameters. Large-eddy simulations show that many of the well-known properties of the cumulus-topped boundary layer (including a well-mixed subcloud layer, a cloud-base transition layer, a conditionally unstable cloud layer, and an inversion layer) emerge naturally in the simulations. The simulations also quantify the differences between nonprecipitating moist convection and its dry counterpart. Whereas dry penetrative convective layers grow proportionally to the square root of time (diffusively) the cumulus layers grow proportionally to time (ballistically). The associated downward transport of warm, dry air results in a significant decrease in the surface Bowen ratio. The linear-in-time growth of the cloud layer is shown to result from the transport and subsequent evaporation of liquid water into the inversion layer. This process acts as a sink of buoyancy, which acts to imbue the free troposphere with the properties of the cloud layer. A simple model, based on this mechanism, and formulated in terms of an effective dry buoyancy flux (which is constrained by the subcloud layer's similarity to a dry convective layer), is shown to provide good predictions of the growth of the layer across a wide range of governing parameters.

1. Introduction

What sets the depth of layers of shallow cumulus convection? The rate at which such layers deepen determines the rate at which dry free-tropospheric air is mixed to the surface, and hence the surface fluxes. The deepening rate also helps determine the time of onset of precipitation, which is closely tied to the depth of the cloud layer (Byers and Hall 1955). The impact of cumulus convection on surface fluxes has been shown to significantly affect larger-scale circulations and the skill of medium-range weather forecasts (Tiedtke 1989). The modulating effect of cloud-layer depth on precipitation may be important to the diurnal cycle of convection over land (Khairoutdinov and Randall 2006) as well as aerosol effects on clouds (Albrecht 1989). In addition, layers of fair-weather cumuli, such as those found in the trades, are increasingly being recognized as a key point of departure among models of the climate system, with much of the variance in model-based estimates of climate sensitivity being attributed to differences in the modeled response of layers of shallow convection (Bony and Dufresne 2005; Wyant et al. 2006).

The question of the growth of layers of shallow, nonprecipitating, cumuli has long been phrased in terms of the maintenance of the trade wind layer. In addressing this very question, Riehl et al. (1951) write:

> It is well known that the bases of the cumuli have a nearly uniform height, but that the tops are very irregular. Some are found within the cloud layer, many near the inversion base, and some within the inversion layer as active clouds penetrate the base. As shown by visual observation and many photographs, the tops of these clouds break off and evaporate quickly. In this way moisture is introduced into the lower portions of the inversion layer, and the air there situated gradually takes on the characteristics of the cloud layer.

Their findings, as embodied by this quote, helped establish the view that the cumulus-induced transport (and subsequent evaporation) of liquid water into the trade wind inversion layer is the principal mechanism counteracting the drying and warming that accompanies the prevailing subsidence. Riehl et al.'s point of view, based on budget analyses of the trade winds of the

Corresponding author address: Bjorn Stevens, Department of Atmospheric and Oceanic Sciences, University of California, Los Angeles, 405 Hilgard Ave., Box 951565, Los Angeles, CA 90095-1565.
E-mail: bstevens@atmos.ucla.edu

DOI: 10.1175/JAS3983.1

northeast Pacific, received further support from similar analyses of data collected as part of the Atlantic Tradewind Experiment (ATEX; Augstein et al. 1973) and Barbados Oceanographic and Meteorological Experiments (BOMEX; Nitta and Esbensen 1974).

These ideas were put in a theoretical context by Betts (1973), whose model of the cumulus layer was based on the budgets of enthalpy in two sublayers: an upper, stably stratified, inversion layer, identified with divergence in the enthalpy flux, net evaporation, and cooling; and a lower, conditionally unstable, cloud layer, identified with a convergent enthalpy flux, net condensation, and warming. Betts showed how this enthalpy flux is largely carried by the transport of liquid water, which is condensed at one level (the cloud layer), and evaporated at another (within the inversion), thus cementing the conceptual foundations of the earlier budget studies.

So while it has long been appreciated, at least by some, that the maintenance of the trades depends on the transport of liquid water, this view is worth contrasting with ideas used to explain the growth, or maintenance, of layers maintained by other types of shallow convective. Dry convective boundary layers are generally understood to deepen as a result of turbulent convective eddies working against the stratification of the capping layer. Simply put, the growth rate dh/dt is expressed as the ratio between the entrainment buoyancy flux, $\mathcal{B}_h$, and the jump in buoyancy, Δb, across the capping layer. Here $\mathcal{B}_h$ measures the rate at which turbulence energy is converted to potential energy, and Δb measures the stability of the interface. (Throughout we use subscript h and 0 to denote inversion and surface values of quantities that vary with height.) For idealized situations this leads to the familiar hypothesis wherein the rate of working against the overlying stratification (the buoyancy flux at the top of the layer) is set to a fixed fraction, k, of the surface driving (as measured by the surface buoyancy flux, $\mathcal{B}_0$) of the layer, that is,

$$\mathcal{B}_h/\mathcal{B}_0 = k. \tag{1}$$

The entrainment flux ratio, k, is taken to be a universal constant (Ball 1960; Betts 1973; Tennekes 1973; Deardorff 1974) that observations, experiments, or simulations attempt to deduce, with $k = -0.2$ being a common reference.

This buoyancy point of view, which emphasizes exchanges between turbulence kinetic and mean flow potential energy, also colors our view of the growth of stratocumulus-topped boundary layers. Most parameterizations strive to represent the growth of the layer by constraining the rate of working at cloud top to the net rate of buoyancy production, due to either radiative cooling, or surface fluxes, within the layer (Turton and Nicholls 1987; Stevens 2002). Such a way of thinking about the energetics of a growing boundary layer is also evident, at times, in discussions of layers maintained by cumulus convection. For instance, Wyant et al. (1997) emphasize this analogy and define an entrainment mass flux based on the relative energetics of cumulus updrafts and the stability of the inversion. This results in an entrainment law similar to (1).

In an attempt to reconcile the thermodynamic point of view of the earlier studies, with the energetic point of view manifest in discussions of the growth of layers maintained by other forms of shallow convection, we revisit the question of the growth of the trade wind layer. Our analysis is centered around large-eddy simulations of an idealized, or prototype, trade wind cumulus layer. Although most studies of trade wind convection are based on abstractions of observed cases (e.g., Sommeria 1976; Nicholls and LeMone 1980; Siebesma and Cuijpers 1995) we focus on an idealized case in an effort to limit the number of parameters on the one hand, and help extract essential phenomena on the other. Such an approach, both common and illustrative in studies of deep precipitating convection (Held et al. 1993; Emanuel and Bister 1996; Tompkins and Craig 1998; Pauluis and Held 2002), is beginning to be used more often in studies of shallow convection (Grant and Brown 1999; Grant 2001). The remainder of this paper is organized as follows: The idealization we explore is described in section 2, and large-eddy simulations thereof are presented in section 3. Section 4 interprets the energetics of the simulations. In section 5 we discuss some of the issues raised by this analysis, including its relation to previous work, and implications for ongoing studies. Section 6 concludes with a brief summary of our major findings.

2. Setup

a. Background

The initial value problem consisting of a uniformly stratified fluid evolving under the action of a constant surface buoyancy flux is perhaps the simplest representation of the dry convective boundary layer. It shall serve as the basis for our study of the effects of cumulus convection and thus merits a brief review. Other than parameters describing the properties of the working fluid, the only parameters in this problem are the stratification, which is measured by the Brunt–Väisälä frequency, N^2, the surface buoyancy flux denoted by $\mathcal{B}_0$, and the time, t, since initialization. It follows dimensionally that the growth law (1) describes the evolution of a mixed layer growing at the same rate as the con-

vective layer, so long as the evolution of the layer is independent of the Prandtl and Reynolds number and $(tN)^{1/3}$. The latter is a nondimensional measure of the ratio of a convective time scale to a gravity wave time scale within the stratified layer and might be expected to measure the importance of energy radiation by waves in the free troposphere. In this limit, the thickness of the inversion layer; that is, that layer whose stratification is greater than the background fluid and is often associated with the presence of penetrative convection, can be shown to scale with the depth of the convecting layer. And so the growth of boundary layer as a whole (irrespective of whether or not is well mixed) can be parameterized by a model consisting of only a single length scale, for example, a simple, or zeroth-order, mixed layer. For such a model it also follows that the depth of the mixed layer, h_m, is given for all time by

$$h_m = \alpha h_* \quad \text{where} \quad h_* = \left(\frac{2\mathcal{B}_0 t}{N^2}\right)^{1/2} \quad \text{and}$$

$$\alpha = \sqrt{1 - 2k}. \tag{2}$$

The scale height h_* is, by assumption, the only length scale in the problem. It is determined by the external parameters and is often called the encroachment depth (e.g., Carson and Smith 1974; Driedonks 1982; Fedorovich 1998) as it describes the growth rate of the layer in the absence of penetrative convection and when an inversion layer is not readily evident. For this case $k = 0$ equivalently $\alpha = 1$. The salient aspect of (2) is that it predicts a scaling regime in which $h \sim t^{1/2}$.

Figure 1 shows both the initial profile and the simulated boundary layer structure from a large-eddy simulation for this initial value problem. Although not shown, it turns out that the growth law (2) is well satisfied by this simulation. Here the height, h_m, of the mixed layer used to scale the growth of the actual convective layer is determined by matching the enthalpy of the two layers within the warmed layer, subject to the overall constraint of enthalpy conservation. Different choices for the mixed layer height, such as the height of the minimum buoyancy flux, $h_{\mathcal{B}}$, or the height of the maximum buoyancy gradient h_θ, would lead to slightly different values of k.[1]

b. Prototype problem

To understand how cumulus convection affects the evolution of the developing thermal boundary layer we extend the canonical problem of the dry convective boundary layer to include clouds. To do so, we propose the modified initial value problem illustrated by Fig. 2. This figure shows a growing and moistening thermal boundary layer at two times, before (dashed lines) and after (dotted lines) the development of clouds. The initial conditions are shown by the solid gray lines. In analogy to the dry convective boundary layer, the modified problem consists of the growth of a thermodynamic boundary layer into a layer whose density is uniformly stratified over a saturated water surface. The surface temperature is varied to maintain a constant surface buoyancy flux, $\mathcal{B}_0$, which is the only source of driving of the flow. Given this basic framework the only unconstrained aspect of the problem is the specification of the initial humidity profile. Ideally, one would like a profile that allows the cloud layer to develop over a reasonable range of heights, and permits its development thereafter to proceed in some statistically invariant manner. The profile chosen with these ideas in mind is the following:

$$q_i(z) = q_{0,+} \exp(-z/\lambda) \cdot \tag{3}$$

It corresponds to a relative humidity profile that decreases exponentially with height. Equation (3) also ensures that the initial equivalent potential temperature, $\theta_e \approx \theta \exp[q_v L/(c_p T)]$, decreases with height. Such a negative gradient in θ_e is both a realistic representation

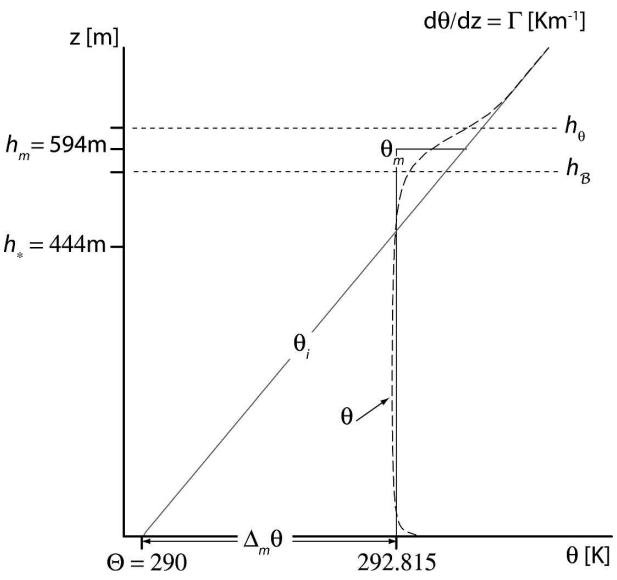

FIG. 1. Development of a convective boundary layer under the action of a constant surface enthalpy flux $\rho_0 c_p Q_0$. Shown are the initial profile θ_i (gray solid line); the profile calculated using LES at $t = 48\,000$ s (dashed line); and equivalent mixed layer profile, θ_m (dark solid line). Also shown are the four heights, h_*, $h_{\mathcal{B}}$, h_m, and h_θ, described in the text.

[1] The fact that k depends on how the layer's depth is defined underscores the point that it does not measure the ratio of the actual minimum buoyancy flux to the surface buoyancy flux, but rather that value required by a mixed-layer model to match the growth of the actual layer (cf. Deardorff et al. 1974).

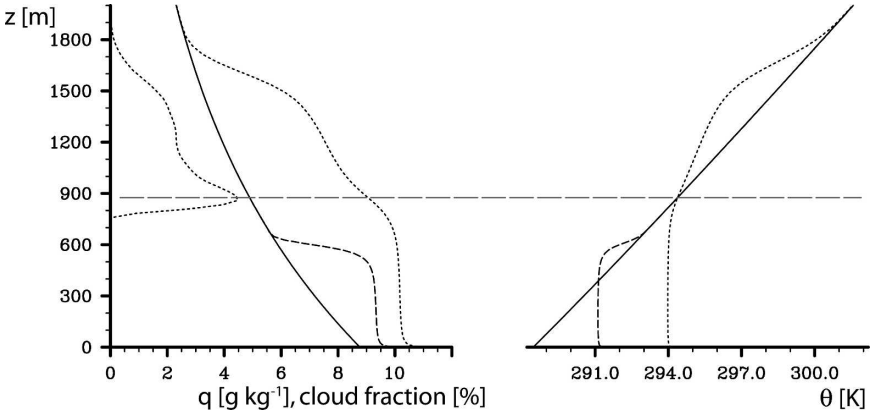

FIG. 2. Development of a moist thermal layer under the action of a constant surface buoyancy flux $\mathcal{B}_0 \simeq 7 \times 10^{-4}$ m^2 s^{-3}. Shown are the initial profiles of θ_i, q_i (solid); and the profiles of θ and q calculated using LES at $t = 24\,000$ s (dashed) and $t = 96\,000$ s (dotted). At the latter time, the cloud fraction is also plotted on the left. Other parameters for this problem include $\lambda = 1500$ m, $q_{0,+} = 0.8q_{s,0}$, and $\Gamma = 6 \times 10^{-3}$ K m^{-1}.

of the lower tropical troposphere, as well as a necessary condition for the growth of a conditionally unstable cloud layer.

Our extension of the canonical problem of the growth of the dry convective boundary layer to allow for cumulus convection introduces three additional parameters (not including microphysical, radiative, or diffusive parameters). These being the two parameters, λ and q_0, introduced explicitly by (3) as well as the moisture scale height

$$\lambda_0 = \frac{R_v c_p \Theta^2}{Lg}, \tag{4}$$

which depends on Θ. The other constants have their usual meanings and are defined in Table 1.

Our motivation for fixing $\mathcal{B}_0$ is twofold: it maintains continuity with the standard representation of the dry convective layer, which simplifies the dynamics of the subcloud layer; and it allows the surface fluxes to be represented by a single parameter. This means that the surface Bowen ratio $\beta \equiv c_p \mathcal{Q}_0/(L\mathcal{R}_0)$, where $\mathcal{Q} \equiv \overline{w'\theta'}$ and $\mathcal{R} \equiv \overline{w'q'}$ is free to vary. We relate the surface fluxes, $\mathcal{Q}_0$ and $\mathcal{R}_0$, to the near surface thermodynamic state as

$$\mathcal{Q}_0 = V(\theta_0 - \theta_{0_+}) \quad \text{and} \quad \mathcal{R}_0 = V(q_0 - q_{0_+}). \tag{5}$$

Both θ_0 and q_0 are determined by the surface temperature and pressure, assuming saturation to determine q_0; θ_{0_+} and q_{0_+} correspond to the thermodynamic state just above the surface; and V is a constant set to 0.01 m s^{-1}.

Some insight into the behavior of the moist system can be obtained by first studying how a mixed layer would evolve if it deepened following (2). In this case, the mixed layer profiles, θ_m and q_m, must evolve in a way that satisfy their respective conservation laws, namely,

$$h_m\theta_m = \int_0^{h_m} \theta_i\, dz + \int_0^t \mathcal{Q}_0\, dt \tag{6}$$

$$h_m q_m = \int_0^{h_m} q_i\, dz + \int_0^t \mathcal{R}_0\, dt. \tag{7}$$

Given q_m, θ_m, and the surface pressure p_0 we can calculate the lifting condensation level, $\eta(t)$. So long as $h_m < \eta$, one would expect the mixed layer representation of the flow evolution to be qualitatively correct. Thereafter the solutions can be expected to increasingly depart from the actual evolution of the layer, as the assumption of a mixed layer evolution implicit in (6)–(7) and the growth law (2) fails to account for the effects of clouds.

The evolution of h_m and η, as predicted by the mixed layer model is shown in the left panel of Fig. 3. Because of the temporal evolution of $\mathcal{Q}_0$ and $\mathcal{R}_0$ the integrals are evaluated numerically with $\alpha = 1.3$, $\Gamma = 6 \times 10^{-3}$ K m^{-1}, and $\mathcal{B}_0 = 7 \times 10^{-4}$ m^2 s^{-3}. Here we note that η equilibrates relatively quickly and h_m grows steadily in time, following the $t^{1/2}$ rule as prescribed by (2). Eventually h_m exceeds η, and clouds are predicted to develop with bases near 600 m after about 8 h. These key features, cloud-base height and cloud onset time are shown as a function of $\mathcal{B}_0$ and λ in the right panel of the same figure. Cloud onset time is most strongly determined by λ through its regulation of η, while the height at which $h_m = \eta$ depends on both λ and $\mathcal{B}$. We note that realistic cloud-base heights (500–700 m being a good

TABLE 1. List of symbols.

a_1	$\partial\theta_\rho/\partial\theta_l$
a_2	$(R_v/R_d - 1)$
a_3	$\theta^{-1}\partial\theta_\rho/\partial_q q_l$
c_p	Isobaric specific heat
g	Gravitational acceleration
t	Time
h	PBL height
h_*	Encroachment depth
$h_{\mathcal{B}}$	Height where $\mathcal{B}$ is a minimum
h_θ	Height where $d\theta/dz$ is a maximum
h_m	Equivalent mixed layer depth
k	Dry convective boundary layer entrainment/surface flux ratio
p	Pressure
q	Total water specific humidity
q_l	Liquid water specific humidity
w	Vertical velocity
z	Distance from surface
z_a	Base of cloud-top interfacial layer
z_b	Top of cloud-top interfacial layer
N^2	Brunt–Väisälä frequency
V	Surface exchange velocity
L	Enthalpy of vaporization
R_d	Gas constant for dry air
R_v	Gas constant for water vapor
T	Temperature
$\mathcal{B}$	Buoyancy flux
$\mathcal{Q}$	Kinematic flux of potential temperature
$\mathcal{Q}_l$	Kinematic flux of liquid water potential temperature
$\mathcal{Q}_\rho$	Kinematic flux of θ_ρ
$\tilde{\mathcal{Q}}_\rho$	Equivalent flux of θ_ρ
$\mathcal{R}$	Total water specific humidity flux
$\mathcal{R}_l$	Liquid water specific humidity flux
β	Surface Bowen ratio
η	Cloud-base height
κ	Nondimensional entrainment of cumulus-topped PBL
λ	Moisture length scale for initial profile
λ_0	Moisture scale height
Θ	Potential temperature at $z = 0$, $t = 0$ (also basic state value of θ)
θ	Potential temperature
θ_e	Equivalent potential temperature
θ_s	Saturated equivalent potential temperature
θ_l	Liquid water potential temperature
θ_ρ	Density potential temperature
$\Delta\theta$	Difference in θ (or perhaps other variable) across the inversion
Γ	$d\theta_\rho/dz$ in free troposphere
Γ_c	$d\theta_\rho/dz$ in cloud layer

tropical rule of thumb) are evident over much of the parameter space.

Because the prediction of the mixed layer model, given by (6)–(7) with (2), does not incorporate cloud processes, it provides a reference for measuring how the development of the cloud layer in the large-eddy simulations (which do incorporate cloud processes) affects the evolution of the boundary layer as a whole, and how this varies as a function of the major parameters of the system. Already from Fig. 2, in which the profiles of θ and q are taken from the large-eddy simulations to be presented subsequently, one can deduce that clouds must have some effect. Whereas (2) would have predicted the boundary layer depth to have doubled in the period between 24 000 and 96 000 s, its actual depth has almost tripled. Using large-eddy simulation as a proxy for the evolution of actual clouds, our goal in the following sections is to better understand this underlying tendency of the clouds to accelerate the growth of the boundary layer.

3. Large-eddy simulations

a. Large-eddy simulation model

The code used to perform the large-eddy simulations is presented in some detail in the appendix of Stevens et al. (2005). Here we briefly summarize by noting that it solves the anelastic equations[2] of Ogura and Phillips (1962) over three spatial dimensions. Centered differences in space and time are used to represent momentum advection, and monotone-centered-slope-limited upwinding is used for the advection of scalars. The Smagorinsky subgrid model is employed to represent subgrid fluxes of both scalars and momentum. The prognostic model variables are the three components of the velocity vector, the liquid-water potential temperature, $\theta_l = \theta \exp[-q_l L/(c_p T)]$ introduced by Betts (1973), and the total water mixing ratio, q. Liquid water, q_l, is diagnosed assuming equilibrium conditions and no rain is allowed to develop. As we shall discuss later, this latter assumption becomes increasingly untenable as the cloud layer deepens.

The model is initialized with a horizontally homogeneous mean state and no mean wind. To specify an initial state of constant N^2, $\theta_i(z)$ is calculated based on $q_i(z)$. To break the slab symmetry of the initial conditions random fluctuations are added to the potential temperature field near the surface. The model is then stepped forward in time, with the sea surface temperature held homogeneous over the domain, but varying in time so as to maintain $\mathcal{B}_0$ at the desired mean value given (5), with θ_{0_+} and q_{0_+} given by their values at the first model level above the surface. Eleven simulations are analyzed, most on a grid whose horizontal spacing is

[2] The analysis of our simulations is performed in a way that accounts for the fact that the background density varies with height. For ease of exposition however the results have been presented in the Boussinesq limit. Throughout we have checked our analysis to ensure that it is not qualitatively sensitive to the height variations of the background density in the simulations.

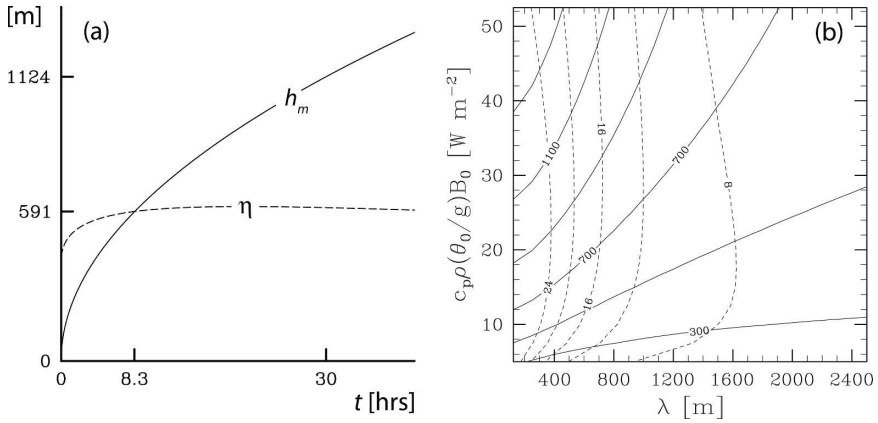

FIG. 3. (left) Time series of h_m (solid) and η (dashed) for a mixed layer growing into a layer with the same initial conditions and surface buoyancy flux as shown in Fig. 2. (right) Cloud-base height, η, (solid contours) and cloud onset time in h (dashed) as a function of $\mathcal{B}_0$ and λ for $k = 1.3$.

75 m and whose vertical grid is 5 m near the surface and stretched by a constant factor of 2.5% per grid interval. This stretching results in a grid spacing of about 30 m near $z = 1200$ m and 120 m near the model top at 4750 m. The standard horizontal domain consists of 96 points in the horizontal and 131 points in the vertical. Simulations on grids twice as large, or twice as fine, suggest that the results we center our analysis around are not especially sensitive to modest changes in the calculation grid, although the larger-domain simulations do yield more reliable statistics at late times in situations when the cloud layer is relatively deep and the finer resolution simulations are more robust at very early times; that is, when $h < 200$ m.

b. Time evolution

In Fig. 4 we show the time evolution of distinguished layers (Fig. 4a) and cloud fractions (Fig. 4b) from a simulation of the prototype problem with the SST chosen so that $c_p\rho_0\Theta g^{-1}\mathcal{B}_0 = 25$ W m^{-2}, $\lambda = 1500$ m, $\Gamma = 6$ K km^{-1}, and $q_0 = 0.8q_{s,0}$. Figure 5 shows the evolution of the sea surface temperature (SST) and surface fluxes from this same simulation.

Two regimes are clearly evident: a cloud-free regime at early times ($t < t_1 = 8.4$ h), and a regime with approximately constant cloud fraction at later times ($t > t_2 = 13$ h). The times t_1 and t_2 are defined when the cloud first exceeds 1% of its value averaged over the final 2 h of the simulation, while t_2 corresponds to the time at which the cloud fraction first exceeds 90% of that value. The time of cloud onset, $t_1 = 8.4$ h is predicted relatively well by the mixed layer equations (which predicted $h_m = \eta$ at 8.3 h). Subsequent to t_2, η tracks $h_{\mathcal{B}}$ (the height of the minimum buoyancy flux) indicating that the latter effectively measures the depth of the subcloud layer at late times. For comparison, we note that the profiles in Fig. 2 are taken from the base simulation at $t = 8$ and $t = 30$ h, respectively.

At early times, that is, $t < t_1$, the boundary layer grows with the square root of time. This is true irre-

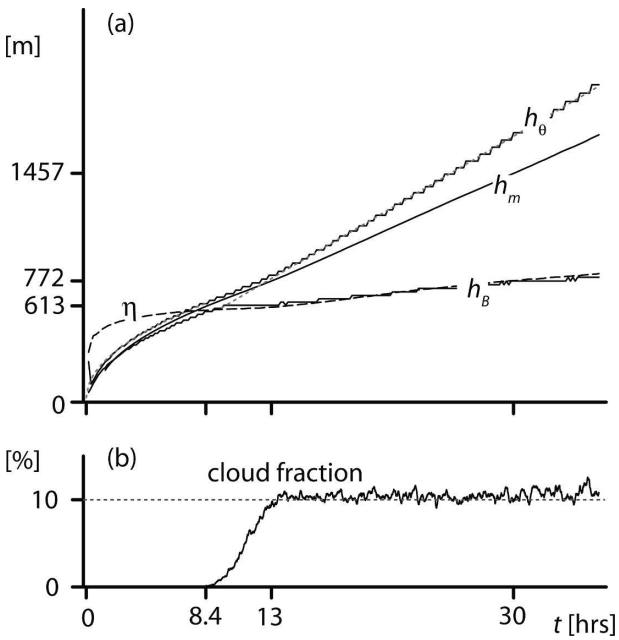

FIG. 4. (a) Time series of distinguished heights for the base simulation described in Fig. 2. A gray dotted line (which is effectively overlaid by other lines) shows the fit to h_θ for $t < 8.4$ h and $t > 13$ h, respectively. The early time fit is proportional to $t^{1/2}$ and the late time fit is proportional to t. Also shown by the dashed line is the lifting condensation level η based on the average value of θ and q over a layer from 0 to $0.2h_{\mathcal{B}}$. (b) Time series of cloud fraction, defined as the percent of columns with condensate.

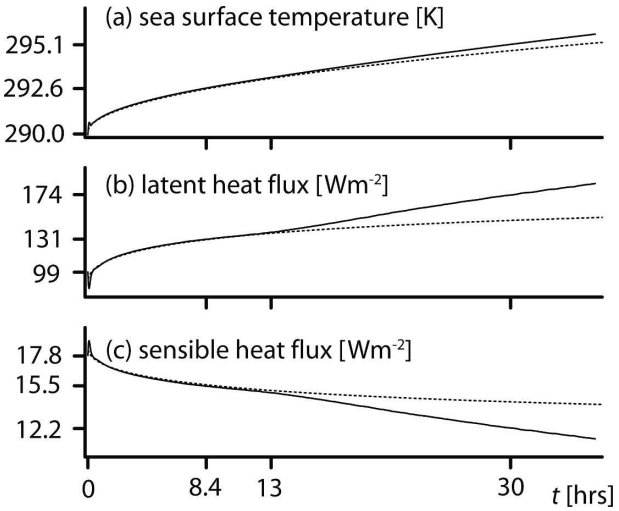

FIG. 5. Time series of (a) sea surface temperature, (b) surface latent enthalpy flux, and (c) surface dry enthalpy flux. Dotted lines are estimates based on bulk model (6)–(7) adjusted to account for the lack of a surface layer in the bulk model, and with h_m given by (2).

spective of how one measures the boundary layer depth, with $h_* < h_{\mathcal{B}} < h_m < h_\theta$ each existing in fixed ratio with respect to one another, especially toward the latter part of the early period when the boundary layer depth is much larger than the grid mesh over which it is represented, that is, $h \gg \Delta x$. By any measure of the layer's depth, $h > h_*$, hence penetrative convection is contributing to the growth of the layer. The signature of penetrative convection is also evident in the development of a thin layer, centered near $h_{\mathcal{B}}$, in which $\theta < \theta_i$. This implies the development of stronger temperature and moisture gradients than were initially present, and is often referred to as an inversion layer because the stratification is sometimes sufficient for the temperature to actually be increasing at h_θ. Because such a layer emerges spontaneously, treating it as a controlling parameter that should be specified externally, as is common practice (e.g., Nieuwstadt et al. 1991; Sullivan et al. 1998), only adds unnecessary complication.

The surface buoyancy flux is calculated as

$$\mathcal{B}_0 = \frac{\theta_0}{g}\left(1 + a_2\frac{c_p T}{\beta L}\right)V(\theta_0 - \theta_{0_+}), \quad \text{where}$$

$$a_2 = \frac{R_v}{R_d} - 1 = 0.608. \tag{8}$$

For fixed β (Bowen ratio) and $\mathcal{B}_0$, the SST (equivalently θ_0) should increase as θ_{0_+} (equivalently θ_m), that is, also proportional to $t^{1/2}$. In Fig. 5 we see that β is decreasing with time, indicating that the SST must increase slightly less rapidly than $t^{1/2}$. The actual time rate of change of the SST and the surface fluxes is predicted by the bulk model to within a constant offset (0.15 K, -9.5 W m^{-2}, and 0.5 W m^{-2} to the SSTs, latent and sensible heat fluxes, respectively), which arises as a result of a surface layer in the simulations. The emergence of such a layer (the precise characteristics of which likely are sensitive to the grid) results in a slightly larger SST and a larger surface Bowen ratio than predicted by (6)–(7) with θ_m and q_m substituted for θ_{0_+} and q_{0_+} in the calculation of the surface fluxes.

At late time, that is, $t > t_2$, the boundary layer enters a qualitatively different scaling regime, wherein we witness the emergence of a cloud layer whose top, h, grows linearly with time, t. This is evident irrespective of how one measures the depth of the layer. At late time the cloud fraction is stationary at about 10% and the SSTs and surface fluxes increasingly depart from what would have been expected had the solutions remained cloud free. In this late time regime, the SST has to increase more markedly to maintain the same buoyancy flux, and the surface Bowen ratio tends to decrease more strongly. The latter is not unlike the evolution of the Bowen ratio along trajectories of low-level winds in the trades (e.g., Riehl et al. 1951) and suggests that our specification of a constant surface buoyancy flux is not unduly artificial. For those readers who are concerned that the rate of increase in the SST in Fig. 5 is unrealistic we note that (i) the actual rate of SST increase, and hence surface buoyancy flux, ends up being immaterial to the arguments we are making; (ii) because we study the problem in the absence of radiative cooling in the atmosphere, for which 2 K day^{-1} is a typical value, it is necessary to increase the surface temperature more rapidly to maintain the same rate of driving of the flow; and (iii) the rate of SST increase implied by the prescribed surface buoyancy flux is varied later in this study thereby substantiating our first point.

The cloud layer at late times (Fig. 2) consists of a deepening layer that has been both cooled and humidified relative to the initial sounding. Cloud fraction peaks at the base of this layer and decreases through the depth of the cooled zone. The capping inversion is now much more pronounced than it was previously and caps a cooled layer that is no longer a well-mixed extension of the lower boundary layer, but follows a conditionally unstable lapse rate, $\Gamma_c \simeq 0.0022$ K m^{-1}. The maximum of cloud fraction near the base of the cloud layer, and the secondary maximum in the gradient of q near 900 m are signatures of a cloud-base transition layer. All of these features are quite realistic, and in accord with the growing body of literature on trade-cumulus convection (see Siebesma 1998; Stevens 2005, for recent reviews). These results also suggest that

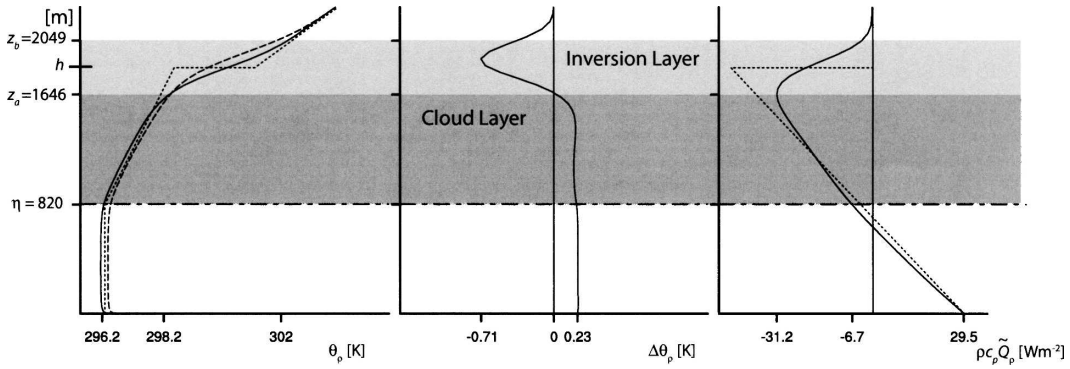

FIG. 6. Density potential temperature, θ_ρ budget: (left) Profiles at 33 h (solid) and 36 h (dashed), and an idealized bulk profile (dotted) based on the average between 33 and 36 h; (middle) difference in θ_ρ between hours 36 and 33; and (right) average of effective θ_ρ flux during 33–36 h.

properties such as the trade inversion, the cloud-base transition layer, and the level of conditional instability in the cloud layer, should be viewed as emergent properties of the simulation, rather than parameters, or boundary conditions, to be specified externally. The merit of this distinction becomes evident when deciding what parameters to use to describe the asymptotic behavior of the layer.

On the basis of this analysis alone, one can begin to glimpse how shallow moist convection changes the world. Trade winds admitting only dry convection would be shallower, and surface heat fluxes would be less, leading to less cooling of the surface ocean, and less charging (moistening) of the atmosphere in anticipation of deep convection (see also Tiedtke 1989; McCaa and Bretherton 2004; Zhu and Bretherton 2004, for similar conclusions). In the next section we will try to put these changes in the theoretical framework sketched out in the introduction.

4. The energetics of the growing cloud layer

Although not shown, the flow visualization suggests that evaporative cooling at the top of the cloud layer may play an important role in the anomalous (t versus $t^{1/2}$) growth of the cloud layer. These images show the now familiar tendency (e.g., Reuter and Yau 1987; Zhao and Austin 2005a,b) of the cumuli to become enveloped, or crowned, by a downdraft sheath as they penetrate and evaporate into the inversion layer. To emphasize the differences between the scaling regimes at early (cloud free) and late times, we borrow from the terminology of stochastic processes and refer to the former as a diffusive, and the latter as a ballistic, growth regime. In this section we focus on the question as to the extent to which the ballistic growth regime is analogous to the growth of dry convective layers, whose anomalous (nonencroachment) growth is supported by the conversion of turbulence kinetic energy into mean-flow potential energy.

a. The energetics of ballistic growth

We begin by considering the budget of buoyancy as measured by the density potential temperature θ_ρ, which following Emanuel (1994) we write as

$$\theta_\rho = \theta\left[1 + \left(\frac{R_v}{R_d} - 1\right)q - \frac{R_v}{R_d}q_l\right]. \tag{9}$$

This differs from the definition of density potential temperature used by Betts and Bartlo (1991), corresponding instead to what they (and others) call the virtual potential temperature for cloudy air. We adopt the Emanuel terminology because the literature is ambiguous as to whether liquid water effects should be included in the virtual temperature, and because θ_ρ makes an explicit reference to the density, differences in which underlies all convection.

The profile of θ_ρ is shown at two different times in Fig. 6. The evolution of the layer is marked by θ_ρ increasing with time in the subcloud and cloud layers, and decreasing with time at the top of the cloud layer: thus defining an inversion layer, which like for the dry convective boundary layer, cools as it deepens. Quantitatively the rate of increase in θ_ρ is remarkably constant through the cloud and subcloud layers (Fig. 6, middle panel). Moreover, as we shall soon show, the rate of warming is commensurate with what one would expect had the subcloud layer been evolving without the subsequent development of clouds.

From (9) and the definition of θ_l, fluctuations in θ_ρ can be linearly related to fluctuations in θ_l, q, and q_l as follows:

$$\theta'_\rho = a_1\theta'_l + a_2\Theta q' + a_3\Theta q'_l, \tag{10}$$

where a_1, a_2, and a_3 are thermodynamic parameters, with a_2 given by (8). If we neglect fluctuations among thermodynamic perturbations, then a_1 and a_3 can also be expressed as effective constants:

$$a_1 = \left(\frac{\Theta_\rho}{\Theta_l}\right)\left(1 + \frac{q_l L}{c_p T}\right)^{-1} \quad \text{and}$$

$$a_3 = a_1\left(\frac{\Theta_l}{\Theta}\right)\frac{L}{c_p T} - \frac{R_v}{R_d}, \tag{11}$$

where Θ_ρ, Θ_l, q_l, and T are taken to be some fixed value representative of the cloud layer. In cumulus layers $q_l \approx 1 \times 10^{-5}$ kg kg^{-1}, so for $\Theta_l \approx \Theta_\rho$, $a_1 \simeq 1$ and $a_3 \simeq L/(c_p T) - R_v/R_d \simeq 7$. At this level of approximation perturbations in θ_ρ are indistinguishable from perturbations in $\theta_{v,l}$ the liquid-water virtual potential temperature (e.g., Emanuel 1994).

Equation (10) provides a basis for studying the budget of buoyancy. By correlating fluctuations in θ_ρ with fluctuations in w it follows that

$$\mathcal{Q}_\rho \equiv \overline{w'\theta'_\rho} = a_1 \mathcal{Q}_l + a_2 \Theta \mathcal{R} + a_3 \Theta \mathcal{R}_l, \tag{12}$$

where $\mathcal{Q}_l$ and $\mathcal{R}_l$ denote the vertical kinematic flux of θ_l and q_l, respectively. This defines the buoyancy flux $\mathcal{B} \equiv (g/\Theta)\mathcal{Q}_\rho$, which measures the exchange between turbulence kinetic and mean-flow potential energy.

To see how the divergence of the buoyancy flux relates to the temporal evolution of buoyancy we recognize that in horizontally homogeneous layers, for which there exist no sources of θ_l or q (i.e., in the absence of radiation and precipitation), then

$$\partial_t \theta_l = -\partial_z \mathcal{Q}_l, \quad \partial_t q = -\partial_z \mathcal{R} \quad \text{and} \quad \partial_t q_l = -\partial_z \mathcal{R}_l + \mathcal{C}, \tag{13}$$

where $\mathcal{C}$ is the net rate of condensation. Associating fluctuations in (10) with changes in time, it follows from above that

$$\partial_t \theta_\rho = -\partial_z \mathcal{Q}_\rho + a_3 \Theta \mathcal{C}. \tag{14}$$

This equation emphasizes that in saturated flows, buoyancy is not conserved—condensation acts as a source term in the buoyancy budget. However, in the case when

$$\partial_t q_l = -\partial_z \mathcal{R}_l + \mathcal{C} \ll \frac{a_1}{a_3 \Theta}\partial_z \mathcal{Q}_l, \tag{15}$$

which in the limit corresponds to q_l being stationary (the case of unsaturated layers being the trivial case), then

$$\partial_t \theta_\rho \simeq a_1 \partial_t \theta_l + a_2 \Theta \partial_t q, \tag{16}$$

which is conserved. Hence, in the stationary limit of q_l, θ_ρ evolves according to

$$\partial_t \theta_\rho = -\partial_z \tilde{\mathcal{Q}}_\rho \quad \text{where} \quad \tilde{\mathcal{Q}}_\rho \equiv a_1 \mathcal{Q}_l + a_2 \Theta \mathcal{R}. \tag{17}$$

It turns out that this flux, $\tilde{\mathcal{Q}}_\rho$, proves central to understanding the energetics of the cloud-layer growth. From (14) and (17) we note that

$$\tilde{\mathcal{Q}}_\rho = \mathcal{Q}_\rho - a_3 \Theta \mathcal{R}_l, \tag{18}$$

which defines $\tilde{\mathcal{Q}}_\rho$, to be proportional to that part of the buoyancy flux not associated with perturbations in q_l. This equation emphasizes the fact that in unsaturated layers $\tilde{\mathcal{Q}}_\rho = \mathcal{Q}_\rho = (\Theta/g)\mathcal{B}$. At a level of approximation commensurate with our determination of the constants a_1 and a_3, $\mathcal{Q}_\rho$ is equivalent to the flux of liquid-water virtual static energy (e.g., Bretherton and Wyant 1997; Bretherton and Park 2007, manuscript submitted to *J. Atmos. Sci.*), while $\tilde{\mathcal{Q}}_\rho$ is what Lewellen and Lewellen (2002) call the "dry" virtual potential temperature flux.

To the extent that the evolution of the cloud layer is well described by (17), which as we show below turns out to be the case, then quasi steadiness[3] implies

$$\partial_t(\partial_z \theta_\rho) = -\partial_{zz} \tilde{\mathcal{Q}}_\rho = 0. \tag{19}$$

In other words, $\tilde{\mathcal{Q}}_\rho$ must be linear. This condition is reasonably well satisfied below the level z_a for the simulation analyzed in Fig. 6. The profile of $\tilde{\mathcal{Q}}_\rho$ in this figure makes two further points: (i) its slope is more or less the same in the cloud and subcloud layer, as we would expect from the fact that the cloud and subcloud layer are warming (as measured by θ'_ρ) at the same rate; and (ii) in the subcloud layer $\tilde{\mathcal{Q}}_\rho$ is indistinguishable from the shape it would assume in the absence of an overlying cloud layer. This latter point is the foundation of almost all models of cumulus convection (e.g., Betts 1973). To the extent that clouds merely act to equilibrate the density of the cloud layer to that of the subcloud layer, which itself evolves according to (1), then

$$\tilde{\mathcal{Q}}_\rho(z) \approx \tilde{\mathcal{Q}}_{\rho,0}\left[1 - (1-k)\frac{z}{\eta}\right] \quad \text{for} \quad z \le z_a, \tag{20}$$

which follows from simple linear extrapolation of $\tilde{\mathcal{Q}}_\rho$ given its surface value $\tilde{\mathcal{Q}}_{\rho,0}$, and its value, $k\tilde{\mathcal{Q}}_{\rho,0}$, at the top of the subcloud layer.

Equation (20) helps explain why the cumulus-topped layer grows more efficiently than the cloud-free convective boundary layer. For both, the divergence of $\tilde{\mathcal{Q}}_\rho$

[3] Recall that in the context of turbulent boundary layers this term refers to the condition that the shape of the profile of a particular quantity does not change in time, that is, stationary gradients.

at $z = h$ drives the growth of the layer. However in cloud-free convective layers $\tilde{Q}_\rho \propto \mathcal{B}$, and thus is energetically constrained to be some fraction of the surface buoyancy flux $\mathcal{B}_0$. This leads to constraints of the form (1). For cloudy layers this energetic constraint is relaxed, for example, Eq. (18), and increasingly negative $\tilde{Q}_\rho$ can be supported by the transport of liquid water in the clouds, thus allowing $\tilde{Q}_\rho$ at h to scale with h, thereby supporting a different (ballistic) scaling regime for the evolution of the layer depth.

These relationships are illustrated in Fig. 7, where we plot the three terms in (18) in buoyancy units. Throughout the cloud layer, $\mathcal{B}$ is nearly constant and significantly smaller than $ga_3\mathcal{R}_l$. In the inversion (between z_b and z_a) $\mathcal{B}$ is nearly zero, and so the divergence of $g/\Theta\tilde{Q}_\rho$ is supported almost entirely by the convergence of the liquid water flux at these levels. This helps quantify the discussion in the introduction, showing that, at least in this prototype problem, the growth of the layer is best interpreted as resulting from the enthalpy of vaporization driving an increase in mean flow potential energy. Unlike in dry layers, the turbulence kinetic energy plays at most an indirect role, in that it supports the circulations that deposit the liquid water in the inversion, and the subsequent mixing that leads to its evaporation.

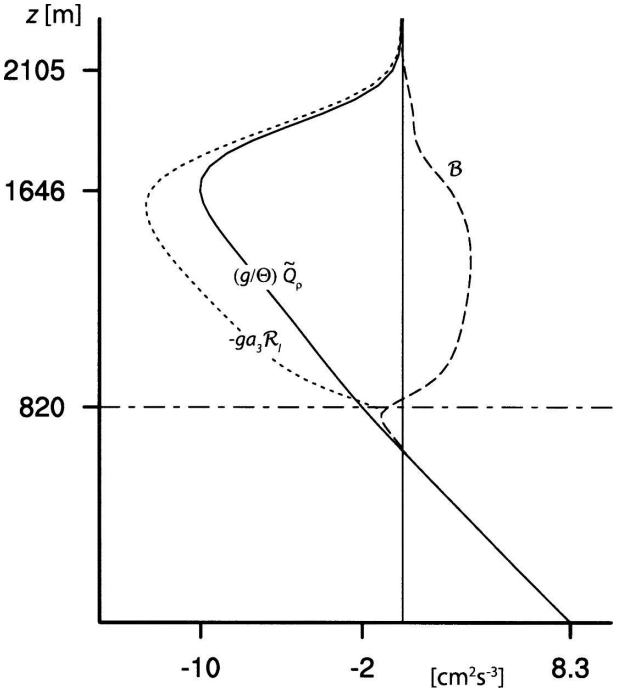

FIG. 7. Fluxes of liquid water (dotted), buoyancy (dashed), and equivalent buoyancy (solid) in buoyancy units for base simulation.

b. Detailed budget

To better quantify these ideas, in this section we examine the budget of the inversion layer in more detail, thus addressing the question as to what role the inversion layer thickness, and the character of the buoyancy jump at cloud top, play in the evolution of the layer.

In the limit where q_l is stationary following the layer, the weak form of the conservation law (14) is given by the integral of (17) between z_a and z_b. Assuming to a first approximation that z_a and z_b evolve at the same rate, so that $dh/dt = dz_a/dt = dz_b/dt$ yields

$$\frac{d}{dt}\int_{z_z(t)}^{z_b(t)} \theta_\rho\, dz \; - \frac{dh}{dt}[\theta_\rho(z_b) - \theta_\rho(z_a)] = \tilde{Q}_\rho(z_a) - \tilde{Q}_\rho(z_b). \tag{21}$$

This equation is the basis for linking flux laws of the form (1) to growth laws of the form (2), but for layers of finite thickness (cf. Sullivan et al. 1998). An analysis of our baseline large-eddy simulation (LES) shows that (21) is satisfied to within 1%, indicating the validity of the assumptions used in its derivation. Assuming that $\tilde{Q}_\rho(z_b)$ is negligible compared to $\tilde{Q}_\rho(z_a)$ and that both terms on the lhs of (21) are proportional to one another; that is,

$$\frac{d}{dt}\int_{z_a(t)}^{z_b(t)} \theta_\rho\, dz - \frac{dh}{dt}[\theta_\rho(z_b) - \theta_\rho(z_a)] \propto -\Delta\theta_\rho \frac{dh}{dt}, \tag{22}$$

allows us to express (21) as

$$-\Delta\theta_\rho \frac{dh}{dt} \propto \tilde{Q}_\rho(z_a). \tag{23}$$

In the dry convective boundary layer, the assumption of a single length scale implies that $\Delta\theta_\rho \propto \Gamma h$ and $\tilde{Q}_\rho(z_a) \approx$ constant, in which case by (23) $hdh \propto dt$ or $h \propto t^{1/2}$ so long as (22) prevails. In contrast, if $\tilde{Q}_\rho(z_a) \propto h$, as we found to be the case for the cumulus-topped boundary layer, then (23) implies that $h \propto t$ so long as $\Delta\theta_\rho$ continues to scale with h.

To further develop these ideas we explore a similarity hypothesis analogous to that used to scale the dry convective boundary layer. Specifically, we hypothesize that an equivalent (bulk) cloud-topped layer of some depth h, consisting of a well-mixed subcloud layer, a cloud layer whose lapse rate Γ_c is constant, and an infinitesimally thin inversion layer[4] deepening under the action of an equivalent θ_ρ flux, $\tilde{Q}_\rho \propto (h - \eta)$, can scale

[4] This fundamentally amounts to assuming that the inversion layer does not introduce a new length scale.

TABLE 2. Summary of simulations.

$(c_p\rho\Theta g^{-1})\mathcal{B}_0$ (W m^{-2})	Γ (K km^{-1})	λ (m)	Analysis time (h)	h_θ (m)	η (m)	Γ_c (K km^{-1})	dh_θ/dt (cm s^{-1})	Note
5	6	1500	26	643	324	1.96	0.62	
15	6	1500	26	1121	578	2.04	1.10	
25	6	1500	26	1452	771	2.04	1.38	
25	6	1500	26	1456	748	2.18	1.42	$2N_x$, $\Delta x/2$
25	6	1500	34	1905	820	2.35	1.48	$2N_x$
40	6	1500	22	1647	899	2.18	1.87	
25	8	1500	26	1159	680	2.53	1.05	
25	4	1500	22	1826	846	1.92	2.31	
25	6	500	34	1400	926	1.85	1.05	
25	6	1000	26	1298	796	1.99	1.23	
25	6	2000	22	1378	702	2.39	1.38	

the growth of the actual cloud-topped boundary layer as represented by our simulations. An example of such a layer, constructed from the 33–36-h mean profiles of θ_ρ is given by the dotted line in Fig. 6. For such a layer

$$\Delta\theta_\rho = \theta_{\rho,0} + \Gamma h - [\hat{\theta}_\rho + \Gamma_c(h - \eta)] \quad \text{where}$$
$$\hat{\theta}_\rho \equiv \frac{1}{\eta}\int_0^\eta \theta_\rho \, dz \, . \tag{24}$$

By conservation of enthalpy

$$\hat{\theta}_\rho + \frac{\Gamma_c}{2}\left[\frac{(h-\eta)^2}{h}\right] = \theta_{\rho,0} + h\frac{\Gamma}{2} + \tilde{Q}_{\rho,0}\frac{t}{h}, \tag{25}$$

which given Γ_c defines $\hat{\theta}_\rho$. Substituting (20) and (24) into (23) leads to an expression for the growth rate of the cumulus layer,

$$\frac{dh}{dt} = \kappa\left\{\frac{\tilde{Q}_{\rho,0}\left[1 - (1-k)\dfrac{h}{\eta}\right]}{\theta_{\rho,0} + \Gamma h - [\hat{\theta}_\rho + \Gamma_c(h-\eta)]}\right\}, \tag{26}$$

where κ, the nondimensional deepening rate, is a constant that carries the proportionality in (23). An aspect of (26) worth drawing attention to is that the moisture scale height λ in the initial profiles does not appear explicitly in the growth rate. It is implicit in that it helps determine η and may determine the extent to which our assumption (15) remains valid. This suggests that, to the extent (26) adequately describes the growth of the cloud layer, once η is set the amount of moisture in the free troposphere has little effect on the rate of growth of the cloud layer (insofar as precipitation remains unimportant), even if it may end up being important to the ensuing structure of that layer. Numerical integration of (26), with η and k fixed, $\hat{\theta}_\rho$ given by (25) with Γ_c = 2.2 K km^{-1}, and $h = \eta$ as an initial conditions, yields values of h that increase linearly at late times (after a few hours). This result is commensurate with Fig. 4 and suggests that (26) is at least qualitatively correct.

As a quantitative test, we evaluate whether (26) can scale the actual growth rate from a range of simulations chosen to sample the parameter space of the prototype problem, details of which are summarized in Table 2. In Fig. 8 we plot (26) versus the actual deepening rate dh_θ/dt as determined by the best-fit linear slope to h_θ for the period $t > t_2$, which corresponds to the period of stationary cloud fraction in Fig. 4. In evaluating (26) we take $k = -0.3$ from our simulations for the dry convective boundary layer. Figure 8 shows that the actual growth rate of the cloud layer is well predicted (scaled)

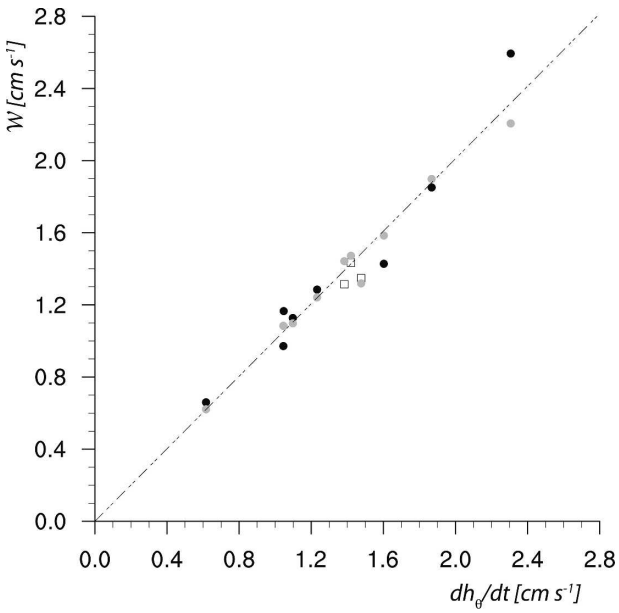

FIG. 8. Predicted vs actual growth rate for simulations in Table 2. The three simulations solved using different numerical formulations (grids) are shown by the open squares. Simulations in which $\mathcal{W}$ is calculated using the actual cloud lapse from each simulation rather than a fixed constant are shown by gray points.

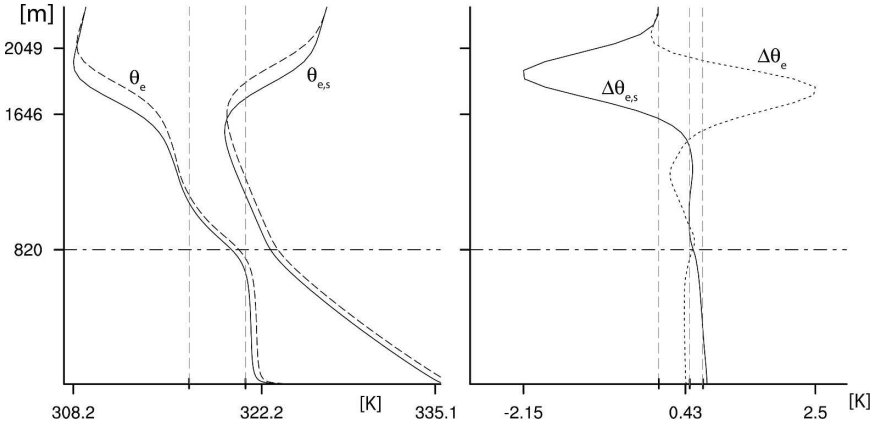

FIG. 9. (left) Profiles of θ_e and θ_s from the base simulation as presented in Fig. 6, and (right) the change in time of θ_e and θ_s.

by (26) given a nondimensional growth rate of $\kappa = 0.8$. The dispersion in k among simulations is only about 10% over a nearly fourfold change in dh_θ/dt. Also evident in this figure is that much of the scatter can be associated with the use of a single value for Γ_c. The lapse rates in the cloud layer vary slightly, but systematically, among the simulations (see Table 2), and unaccounted for variations in Γ_c account for a significant amount of the scatter in the predicted versus the actual growth rates. The variation of κ for the same case, but simulated using different grids and evaluated at different times (marked by open squares), is similar to the variation of κ among simulations with different parameter sets. This suggests that the simulations probably do not sufficiently sample the flow to provide more quantitative information about systematic variations in quantities like the lapse rate or the inversion layer thickness and their effect on the growth of the layer.

In summary, the growth of the cloud layer in this prototype problem is well described by assuming that (i) changes in the cloud water field at a given level contribute negligibly to the evolution of θ_ρ; (ii) the increase in θ_ρ in the cloud layer tracks changes in the subcloud layer; and (iii) the energetics of the subcloud layer are, to leading order, indistinguishable from those of a dry convective boundary layer. The last assumption requires the cloud-base buoyancy flux to be a fixed fraction of its value at the surface, and the first two require the equivalent θ_ρ flux at the top of the cloud layer to scale with the depth of the cloud layer following (20).

5. Discussion

Based on the above, some issues emerge that warrant further discussion. One is why the cloud-layer value of θ_ρ so closely tracks the value in the subcloud layer. Another is how our ideas relate to the significant body of earlier literature that addresses similar topics, and the last is what implications our findings have for ongoing research.

a. Thermodynamic constraints

The first question can be posed formally as follows:

$$\text{Why does } \partial_t \theta_\rho|_{\eta<z<z_a} = \partial_t \theta_\rho|_{z<\eta}? \tag{27}$$

In words: why does the density potential temperature in the cloud layer so closely track its value in the subcloud layer? Perhaps to preserve the stability of the cloud layer with respect to unsaturated perturbations from the subcloud layer? Maintaining the cloud layer at neutral buoyancy with respect to saturated perturbations from the subcloud layer requires that θ_s (the saturated value of θ_e) in the cloud-layer track θ_e in the subcloud layer; that is,

$$\partial_t \theta_e|_{\eta<z<z_a} = \partial_t \theta_s|_{z<\eta}. \tag{28}$$

Figure 9 shows that this constraint is also satisfied by the simulation. Satisfying both the unsaturated (27) and saturated (28) constraints, and assuming that the cloud and subcloud layer are moistening at the same rate, effectively partitions the moisture and heat flux divergences such that

$$\partial_z \mathcal{R} \simeq \frac{qL}{R_v T^2}\, \partial_z Q_l, \tag{29}$$

which upon integrating allows one to differentiate between the heat and moisture fluxes themselves.

b. Relation to previous work

With a little scrutiny the thread of the ideas presented above is apparent in the fabric of much previous work, beginning with that of Betts (1973). While Betts

framed his study around the enthalpy budget of an existing cloud layer, his ideas encapsulate much of the behavior of our prototype problem of a developing convective layer under the action of a fixed surface buoyancy flux. Of the many similarities, his invocation of the assumption that the liquid water is stationary, and the way in which he formulates the problem as an extension of the development of the cloud-free convective boundary layer are especially important. His results also anticipate the linear growth regime, which we highlight in the present work. In particular, the unnumbered equation following his Eq. (62) implies that the cloud layer will grow linearly with time in the case when the inversion layer thickness scales with the depth of the cloud layer as a whole. Although Betts only addresses the stability and energetics of the system as a way to address the question of the inversion layer thickness, some of the similarities in the two studies follow from the fact that the effective buoyancy flux around which we center our analysis so closely tracks the flux of θ_l around which Betts centers his analysis. This follows largely from (17) and (29), which together imply that

$$\partial_z \tilde{Q}_\rho \simeq \left(1 + \frac{a_2 \Theta L q}{R_v T^2}\right) \partial_z Q_l \simeq 1.1 \partial_z Q_l. \qquad (30)$$

In other words, to a first approximation the divergence of the enthalpy (as measured by $c_p \theta_l$) flux is a good approximation to the divergence of the density flux. These similarities necessarily carry over to the finding of Betts (1973, 1975), that the liquid water flux, $\mathcal{R}_l$, is a dominant contributor to the flux of θ_l, and our finding that the $\mathcal{R}_l$ term (e.g., Fig. 7) supports the large downward flux of buoyancy in the cloud layer. The similarity between $\tilde{Q}_\rho$ and Q_l also explains why the scaling of Moeng (2000), which was also based on an analysis of the budget of θ_l, so effectively scaled the growth of the stratocumulus layers she studied.

In their study of different shallow cloud regimes, Lewellen and Lewellen (2002) do focus on the energetics of deepening cloud layers, and in so doing suggest a constraint [their Eq. (10)] essentially identical to our (20) but phrased in terms of what they call D, the buoyancy flux for dry layers. They show its appropriateness for shallow cumulus layers, particularly in so far as they rise into an upper layer of stratocumulus. From this perspective we are simply arguing for the more general validity of their result. In so doing we provide an argument for its interpretation and energetic support (the liquid water flux) especially in layers where the cloud layer is far from uniform (i.e., in situations that violate their assumption 2).

c. Implications for ongoing work

While the linear growth law of the cloud layer will only be realized in the limit of a constant surface buoyancy flux and uniform outer layer stratification, our understanding of why this regime is manifest should also help us understand the behavior of cumulus-topped layers more generally. In particular, because θ_ρ evolves under the divergence of the flux $\tilde{Q}_\rho$, which is closely related to Q_l, both of which must be linear[5] for the quasi-steady evolution of the layer, it is not surprising that arguments based on the enthalpy budget are so successful in describing the boundary layer evolution. More importantly, this suggests that simple models that treat the evolution of the enthalpy budget consistently should be able to well represent the rate of deepening of cloud-topped boundary layers. That said, because the parameter complexity of simple parameterizations (in terms of dimensional constants) often exceeds that of the underlying flow, it is less clear that parameterizations forced under the conditions of this simple problem recover the simple scaling of (26). As such the prototype problem we propose here might prove to be a useful benchmark for parameterization schemes.

A better understanding of the mechanism by which cumulus-topped layers deepen is also useful when thinking about processes that may arrest the ballistic growth of the trade wind layer. These include large-scale subsidence, precipitation, and unfavorable gradients in θ_e. As the cloud layer deepens, precipitation can be expected to become increasingly efficient at depleting the liquid-water flux, and thus arresting the growth of the layer. Preliminary simulations of our prototype case with a simple microphysical scheme (to be discussed further in a subsequent paper) indeed show that as the precipitation rate increases the cloud layer ceases to deepen. These simulations also show that $\Gamma_{c,}$, which is approximately fixed in the nonprecipitating regimes, increases markedly as precipitation increases. Because the depth of the cloud layer necessary to produce a precipitation flux large enough to balance the upward flux of liquid water depends on the ambient concentration of condensation nuclei this suggests yet another mechanism whereby the chemical state of the atmosphere (as measured by the atmospheric aerosol) may affect the structure of larger-scale circulations, and hence climate. The ability of precipitation to quench the growth of the cloud layer may also help explain simulations of stratocumulus whereby increasing pre-

[5] If other sources such as radiation are active, then the linearity constraint of quasi steadiness applies to the sum of the radiative and turbulent fluxes.

cipitation, or sedimentation, fluxes appear to reduce the entrainment rate (e.g., Stevens et al. 1998; Ackerman et al. 2004; Bretherton et al. 2007).

Last, the mechanisms we discuss here suggest a new twist on how we usually view the role of large-scale θ_e gradients (cf. Squires 1958; Randall 1980; Deardorff 1980). For negative θ_e gradients, the ballistic (water injection) growth mechanism provides an efficient means for deepening the boundary layer. In unfavorable θ_e gradients the injection of water into the inversion layer can lessen, but not obliterate, unfavorable density gradients. In the latter case, the rate of working against the outer-layer stratification, by a negative buoyancy flux, is essential to sustain boundary layer growth. Because doing work on the outer-layer stratification proves to be an inefficient way to grow a boundary layer, such situations would appear to be more favorable for moistening the cloud layer and the development of a layer of stratiform clouds at its top.

6. Summary

We have constructed an idealized representation of a shallow cumulus layer to explore how the development of cumulus clouds affects the growth of the PBL. We pose the problem as one of a thermal boundary layer growing into a uniformly stratified layer whose specific humidity decays exponentially. The growth is maintained by the action of a constant surface buoyancy flux, which is specified by assuming a fixed wind speed and a saturated lower boundary whose temperature is allowed to evolve in time.

In the period before clouds develop, the problem is identical to that of a dry convective boundary layer, for which the layer deepens self-similarly with the square root of time. When clouds develop they quickly equilibrate to maintain a constant cloud fraction near 10%, after which the boundary layer deepens at a rate that increases linearly with time (ballistically). The more rapid deepening of the boundary layer enhances the downward mixing of heat and dry air, which by the surface specification implies enhanced moisture fluxes, and diminished surface sensible heat fluxes. Many characteristics of shallow cumulus layers are apparent in this prototype problem. These include a well-mixed subcloud layer, a transition layer (most evident in moisture gradients), a conditionally unstable cloud layer, and an inversion layer into which clouds penetrate and detrain.

The tendency of the cloud layer to grow linearly in time is explained in terms of a mechanism that is fundamentally different than that used to support the growth of dry convective boundary layers. In the cloud-topped layers, the convective clouds penetrate into a conditionally unstable capping layer and detrain (inject) their liquid water there. The subsequent evaporation of which imbues the capping layer with the properties of the cloud layer. This injection mechanism is best measured by what we call the equivalent flux of density potential temperature. Its value at the top of the cloud layer is constrained by the subcloud layer energetics (which are isomorphic to that of a dry convective boundary layer) and the tendency for the cloud layer values of θ_ρ to change commensurately with the values in the subcloud layer. The development of a simple bulk model based on these concepts is shown to provide a satisfactory prediction of the growth rate for a suite of large-eddy simulations configured to sample a wide span of the problem's parameter space.

While we have made progress in understanding a highly idealized problem, one could argue that many of our idealizations are untenable: even shallow clouds can readily develop precipitation, radiative cooling cannot be ignored, nor can the vertical shear in the horizontal wind. And while the trade wind layer tends to advect over steadily warming water, with progressively decreasing Bowen ratios, they probably do not do so at a rate that maintains a constant surface buoyancy flux. As such one might rightly inquire as to the relevance of our arguments. Notwithstanding the simplifications made in framing the problem, to the extent the simulations we describe behave like a real cumulus-topped layer would in a similar situation, we believe that the present study makes a number of fundamental contributions. Foremost, it provides a framework for thinking about more realistic problems, in so doing it clarifies the link between the evolution of the density and enthalpy fields, the latter being the basis of many past studies of trade–cumulus layers. Finally, it defines a useful test problem, and a rich set of constraints that can be used to evaluate and improve more general models (or parameterizations) of shallow convection.

Acknowledgments. The exploration of this problem was motivated by Kerry Emanuel, whose pounding of the projection screen in want of a theory of moist convection during a lecture at the Institute on Pure and Applied Mathematics 2002 summer school motivated me to develop this simple framework. The ideas developed here also benefited greatly from subsequent conversations and comments by Alan Betts, Christopher Bretherton, Kerry Emanuel, Chin-Hoh Moeng, Pier Siebesma, and João Teixeira. Louise Nuijens and Verica Savic-Jovcic are also thanked for their comments on an early version of this manuscript, which

improved the presentation. Computational resources were made available by NCAR. Financial support has been provided by NSF Grants ATM-00342625, ATM-9985413, and NASA Grant NGT5-30499.

REFERENCES

Ackerman, A. S., M. P. Kirkpatrick, D. E. Stevens, and O. B. Toon, 2004: The impact of humidity above stratiform clouds on indirect aerosol climate forcing. *Nature,* **432,** 1014–1017.

Albrecht, B. A., 1989: Aerosols, cloud microphysics and fractional cloudiness. *Science,* **245,** 1227–1230.

Augstein, E., H. Riehl, F. Ostapoff, and V. Wagner, 1973: Mass and energy transports in an undisturbed Atlantic trade wind flow. *Mon. Wea. Rev.,* **101,** 101–111.

Ball, F. K., 1960: Control of inversion height by surface heating. *Quart. J. Roy. Meteor. Soc.,* **86,** 483–494.

Betts, A. K., 1973: Non-precipitating cumulus convection and its parameterization. *Quart. J. Roy. Meteor. Soc.,* **99,** 178–196.

——, 1975: Parametric interpretation of trade wind cumulus budget studies. *J. Atmos. Sci.,* **32,** 1934–1945.

——, and J. Bartlo, 1991: The density temperature and the dry and wet virtual adiabats. *Mon. Wea. Rev.,* **119,** 169–175.

Bony, S., and J.-L. Dufresne, 2005: Marine boundary layer clouds at the heart of tropical cloud feedback uncertainties in climate models. *Geophys. Res. Lett.,* **32,** L20806, doi:10.1029/2005GL023851.

Bretherton, C. S., and M. C. Wyant, 1997: Moisture transport, lower tropospheric stability, and decoupling of cloud-topped boundary layers. *J. Atmos. Sci.,* **54,** 148–167.

——, P. N. Blossey, and J. Uchida, 2007: Cloud droplet sedimentation, entrainment efficiency, and subtropical stratocumulus albedo. *Geophys. Res. Lett.,* **34,** L03813, doi:10.1029/2006GL027648.

Byers, H. R., and R. K. Hall, 1955: A census of cumulus-cloud height versus precipitation in the vicinity of Puerto Rico during the winter and spring of 1953–1954. *J. Meteor.,* **12,** 176–178.

Carson, D. J., and F. B. Smith, 1974: Thermodynamic model for the development of a convectively unstable boundary layer. *Advances in Geophysics,* Vol. 18A, Academic Press, 111–124.

Deardorff, J. W., 1974: Three-dimensional numerical study of the height and mean structure of a heated planetary boundary layer. *Bound.-Layer Meteor.,* **7,** 81–106.

——, 1980: Cloud top entrainment instability. *J. Atmos. Sci.,* **37,** 131–147.

——, E. G. Willis, and D. K. Lilly, 1974: Comments on nonprecipitating cumulus convection and its parameterization. *Quart. J. Roy. Meteor. Soc.,* **100,** 122–123.

Driedonks, A. G. M., 1982: Models and observations of the growth of the atmospheric boundary layer. *Bound.-Layer Meteor.,* **23,** 283–306.

Emanuel, K. A., 1994: *Atmospheric Convection.* Oxford University Press, 580 pp.

——, and M. A. Bister, 1996: Moist convective velocity and buoyancy scales. *J. Atmos. Sci.,* **53,** 1111–1143.

Fedorovich, E., 1998: Bulk models of the atmospheric convective boundary layer. *Buoyant Convection in Geophysical Flows,* E. J. Plate et al., Eds., Vol. 513 of C, Kluwer Academic, 265–290.

Grant, A. L. M., 2001: Cloud based fluxes in the cumulus-capped boundary layer. *Quart. J. Roy. Meteor. Soc.,* **127,** 407–422.

——, and A. R. Brown, 1999: A similarity hypothesis for shallow-cumulus transports. *Quart. J. Roy. Meteor. Soc.,* **125,** 1913–1936.

Held, I. M., R. S. Hemler, and V. Ramaswamy, 1993: Radiative–convective equilibrium with explicit two-dimensional moist convection. *J. Atmos. Sci.,* **50,** 3909–3927.

Khairoutdinov, M., and D. Randall, 2006: High-resolution simulation of shallow-to-deep convection transition over land. *J. Atmos. Sci.,* **63,** 3421–3436.

Lewellen, D. C., and W. S. Lewellen, 2002: Entrainment and decoupling relations for cloudy boundary layers. *J. Atmos. Sci.,* **59,** 2966–2986.

McCaa, J. R., and C. S. Bretherton, 2004: A new parameterization for shallow cumulus convection and its application to marine subtropical cloud-topped boundary layers. Part II: Regional simulations of marine boundary layer clouds. *Mon. Wea. Rev.,* **132,** 883–896.

Moeng, C.-H., 2000: Entrainment rate, cloud fraction, and liquid water path of PBL stratocumulus clouds. *J. Atmos. Sci.,* **57,** 3627–3643.

Nicholls, S., and M. A. LeMone, 1980: The fair weather boundary layer in GATE: The relationship of subcloud fluxes and structure to the distribution and enhancement of cumulus clouds. *J. Atmos. Sci.,* **37,** 2051–2067.

Nieuwstadt, F. T. M., P. J. Mason, C.-H. Moeng, and U. Schumann, 1991: Large-eddy simulation of the convective boundary layer: A comparison of four computer codes. *Turbulent Shear Flows 8: Selected Papers from the Eighth International Symposium on Turbulent Shear Flows,* F. Durst et al., Eds., Springer-Verlag, 353–367.

Nitta, T., and S. Esbensen, 1974: Heat and moisture budget analyses using BOMEX data. *Mon. Wea. Rev.,* **102,** 17–28.

Ogura, Y., and N. A. Phillips, 1962: Scale analysis of deep and shallow convection in the atmosphere. *J. Atmos. Sci.,* **19,** 173–179.

Pauluis, O., and I. M. Held, 2002: Entropy budget of an atmosphere in radiative–convective equilibrium. Part I: Maximum work and frictional dissipation. *J. Atmos. Sci.,* **59,** 125–139.

Randall, D. A., 1980: Conditional instability of the first kind upside-down. *J. Atmos. Sci.,* **37,** 125–130.

Reuter, G. W., and M. K. Yau, 1987: Mixing mechanisms in cumulus congestus clouds. Part II: Numerical simulations. *J. Atmos. Sci.,* **44,** 798–827.

Riehl, H., T. C. Yeh, J. S. Malkus, and N. E. la Seur, 1951: The north–east trade of the Pacific Ocean. *Quart. J. Roy. Meteor. Soc.,* **77,** 598–626.

Siebesma, A. P., 1998: Shallow convection. *Buoyant Convection in Geophysical Flows,* E. J. Plate et al., Eds., Vol. 513 of C, Kluwer Academic, 441–486.

——, and J. W. M. Cuijpers, 1995: Evaluation of parametric assumptions for shallow cumulus convection. *J. Atmos. Sci.,* **52,** 650–666.

Sommeria, G., 1976: Three-dimensional simulation of turbulent processes in an undisturbed trade wind boundary layer. *J. Atmos. Sci.,* **33,** 216–241.

Squires, P., 1958: Penetrative downdraughts in cumuli. *Tellus,* **10,** 381–385.

Stevens, B., 2002: Entrainment in stratocumulus mixed layers. *Quart. J. Roy. Meteor. Soc.,* **128,** 2663–2690.

——, 2005: Atmospheric moist convection. *Annu. Rev. Earth Planet. Sci.,* **33,** 605–643.

——, W. R. Cotton, G. Feingold, and C.-H. Moeng, 1998: Large-eddy simulations of strongly precipitating, shallow, stratocumulus-topped boundary layers. *J. Atmos. Sci.,* **55,** 3616–3638.

——, G. Vali, K. Comstock, R. Wood, M. C. van Zanten, P. H. Austin, C. S. Bretherton, and D. H. Lenschow, 2005: Pockets of open cells and drizzle in marine stratocumulus. *Bull. Amer. Meteor. Soc.,* **86,** 51–57.

Sullivan, P. P., C.-H. Moeng, B. Stevens, D. H. Lenschow, and S. D. Mayor, 1998: Structure of the entrainment zone capping the convective atmospheric boundary layer. *J. Atmos. Sci.,* **55,** 3042–3064.

Tennekes, H., 1973: A model for the dynamics of the inversion above a convective boundary layer. *J. Atmos. Sci.,* **30,** 558–567.

Tiedtke, M., 1989: A comprehensive mass flux scheme for cumulus parameterization in large-scale models. *Mon. Wea. Rev.,* **117,** 1779–1800.

Tompkins, A. M., and G. C. Craig, 1998: Radiative convective equilibrium in a three-dimensional cloud-ensemble model. *Quart. J. Roy. Meteor. Soc.,* **124,** 2073–2097.

Turton, J. D., and S. Nicholls, 1987: A study of the diurnal variation of stratocumulus using a multiple mixed layer model. *Quart. J. Roy. Meteor. Soc.,* **113,** 969–1009.

Wyant, M. C., C. S. Bretherton, H. A. Rand, and D. E. Stevens, 1997: Numerical simulations and a conceptual model of the stratocumulus to trade cumulus transition. *J. Atmos. Sci.,* **54,** 168–192.

——, ——, J. T. Backmeister, J. T. Kiehl, I. M. Held, S. A. Klein, and B. J. Soden, 2006: A comparison of low-latitude cloud properties and their response to climate change in three AGCMs sorted into regimes using mid-tropospheric vertical velocity. *Climate Dyn.,* **27,** 261–279.

Zhao, M., and P. H. Austin, 2005a: Life cycle of numerically simulated shallow cumulus clouds. Part I: Transport. *J. Atmos. Sci.,* **62,** 1269–1290.

——, and ——, 2005b: Life cycle of numerically simulated shallow cumulus clouds. Part II: Mixing dynamics. *J. Atmos. Sci.,* **62,** 1291–1310.

Zhu, P., and C. S. Bretherton, 2004: A simulation study of shallow moist convection and its impact on the atmospheric boundary layer. *Mon. Wea. Rev.,* **132,** 2391–2409.